



Article

Influences of a Highly Reflective Mulching Membrane on Heat Propagation throughout the Soil

Mattia Manni ^{1,*} , Alessia Di Giuseppe ¹, Andrea Nicolini ² , Fabio Scieurpi ³ and Franco Cotana ²

¹ Interuniversity Research Center on Pollution and Environment “Mauro Felli”, 06125 Perugia, Italy; alessia.digiuseppe@crbnet.it

² Department of Engineering, University of Perugia, 06125 Perugia, Italy; andrea.nicolini@unipg.it (A.N.); franco.cotana@unipg.it (F.C.)

³ Department of Architecture, University of Florence, 50121 Florence, Italy; fabio.sciurpi@unifi.it

* Correspondence: manni@crbnet.it

Abstract: Agro-food chain impacts global greenhouse gas emissions by around 30%. To reduce this score without worsening food crops’ yield, new and more sustainable technologies (i.e., mulching membranes, advanced irrigation systems) were implemented. Within this framework, the present study aims to assess the influences on heat propagation throughout the soil of a highly reflective mulching membrane. An experimental facility was implemented in which the surface temperatures of both the soil and the membrane were monitored together with the temperature of the soil (at three depths). Five statistical days were defined by considering the same amount of percentiles of the monitored temperatures (0th, 25th, 50th, 75th, and 100th percentiles). Then, the attenuation and the phase shift of the thermal wave throughout the soil and the cooling potential of the membrane were calculated. Although negligible variations from the uncovered soil were observed in surface temperature, the membrane enables a greater attenuation of the thermal wave throughout the soil. This can be up to 16 °C cooler than the surface, with potential benefits for plant growth. Furthermore, the membrane optical properties permit to offset carbon emissions from agriculture activities by around 0.1 tCO_{2-eq} m⁻².

Keywords: cool materials; sustainable agriculture; monitoring campaign



Citation: Manni, M.; Di Giuseppe, A.; Nicolini, A.; Scieurpi, F.; Cotana, F. Influences of a Highly Reflective Mulching Membrane on Heat Propagation throughout the Soil. *Sustainability* **2021**, *13*, 9737. <https://doi.org/10.3390/su13179737>

Academic Editor: Michael S. Carolan

Received: 30 June 2021

Accepted: 27 August 2021

Published: 30 August 2021

Publisher’s Note: MDPI stays neutral with regard to jurisdictional claims in published maps and institutional affiliations.



Copyright: © 2021 by the authors. Licensee MDPI, Basel, Switzerland. This article is an open access article distributed under the terms and conditions of the Creative Commons Attribution (CC BY) license (<https://creativecommons.org/licenses/by/4.0/>).

1. Introduction

The rising of urban air temperature, as well as the increasing frequency of extreme events such as periods of droughts and flooding events, are the most evident consequences of currently ongoing climate changes [1]. Anthropogenic warming reached 1.2 ± 0.1 °C above pre-industrial levels in 2020 [2], and the overwarming phenomenon already represents a critical issue for at least 40% of the global population. National governments promoted agricultural and economic policies and measures for mitigating the amount of greenhouse gases (GHG) that are released in the atmosphere, to reduce the frequency of such disaster events. However, the GHG emission trend projections highlighted that current policies and measures will probably fail to achieve the 40% reduction target (from 1990 levels) which was set for 2030 [3] if no additional measures are implemented.

Although agriculture has significantly reduced its environmental impact since the 1990s, it is the sixth most impacting sectors in Europe [3]. Agro-food chains impact global GHG emissions by around 30% [4]. At the same time, climate changes negatively affect agricultural activities causing a reduction in crop productivity and significant economic losses [5–7]. Therefore, several studies in the literature have assessed the environmental impact of various food crops with the aim of reducing GHG emissions from agriculture through a sustainable diet. Roots such as onions (0.17 kgCO_{2-eq} kg⁻¹), potatoes (0.18 kgCO_{2-eq} kg⁻¹), and carrots (0.20 kgCO_{2-eq} kg⁻¹) showed the lowest GHG emissions amount along with vegetables (0.37 kgCO_{2-eq} kg⁻¹) and fruits (0.42 kgCO_{2-eq} kg⁻¹), while

seeds such as sunflowers ($1.41 \text{ kgCO}_2\text{-eq kg}^{-1}$) were characterized by the greatest environmental impact together with wheat and pulses (around $0.50 \text{ kgCO}_2\text{-eq kg}^{-1}$) [4,8,9]. Conversely, other studies focused on agriculture techniques that can be responsible for the production of large volumes of GHG.

Within this framework, new and more sustainable technologies such as mulching membranes, advanced irrigation systems, water recovery plants, and high-efficiency greenhouse infrastructures were implemented to further enhance the growth process and the yield of food crops, while reducing their ecological footprint [10–12]. Highly reflective materials that had been demonstrated to be a valid solution to reduce global temperature [13], were proposed for the agricultural sector [14]. Their cooling potential was assessed at various latitudes [15–17]. When exploited on buildings' envelope, they generally contribute to lowering the energy consumption throughout the year [18]. However, their exploitation in densely built environments showed drawbacks such as the increasing of inter-building reflections [19,20]. Increased materials' reflectance may lead to the increment of solar irradiation amounts trapped in the urban corridors through multiple reflections, thus worsening the cooling effects from highly reflective materials. These treated surfaces reflect solar irradiation in a Lambertian diffuse way by orienting the reflected fraction mainly toward the closest buildings. To overcome this limitation, retro-reflective materials were introduced as a sub-group of the highly reflective ones [21]. Such materials couple the high solar reflectance coefficient to the capacity of directing the reflected rays toward the source and beyond the urban canyon boundaries. However, benefits due to retro-reflective materials are less evident when this coating is applied to a horizontal surface within a low-density built environment, such as the application considered in this study.

Thus, this study aims at investigating the influences on heat propagation throughout the soil of a system based on highly reflective materials coupled to a traditional mulching membrane. Generated knowledge about soil temperatures will permit a selection of adequate food crops to be cultivated in the next stage of the research project. An experimental facility was implemented in the university campus of the Department of Engineering, in Perugia. The thermal attenuation and the phase shifting of the thermal wave throughout the soil, together with the membrane's cooling potential, were evaluated for five statistical days. Moreover, carbon emissions compensated by the mulching membrane due to the highly reflective layer were quantified.

The paper is structured as follows: an introductory section (Section 1) that describes the problem statement and the research core; a Materials and Methods section (Section 2) articulated around five sub-sections and defining the followed workflow (Section 2.1), the material's optical characterization (Section 2.2), the experimental facility (Section 2.3), the layout of the sensors and the data collection phase (Section 2.4), and the data post-processing (Section 2.5); a Results section (Section 3), where the optical properties of the membrane (Section 3.1) and the data from the monitoring campaign (Section 3.2) are presented along with the statistical analysis and the key performance indicators (Section 3.3); a Discussion section (Section 4) where results are interpreted together with the future developments; and finally a Conclusions section recapitulating the results and the implications of this work (Section 5).

2. Materials and Methods

2.1. Workflow

The workflow followed in the hereby study is articulated into four main stages such as (a) optical characterization of the membrane, (b) experimental field setup, (c) data collection, and (d) data post-processing and analysis.

The material characterization (stage a) was conducted on a sample of the highly reflective mulching membrane provided by an Italian company. The optical parameters investigated were the spectral reflectance, the spectral emittance, and the solar reflectance index (SRI). During *stage b*, the highly reflective mulching membrane was applied to the experimental field in Perugia, Italy. Two configurations were investigated: the soil was

covered by the membrane in the first scenario (*enhanced scenario*), and it was uncovered in the second (*reference case*). No food crop was cultivated to avoid shadowing phenomena and evapotranspiration effects from vegetation that might compromise the estimation of the membrane's cooling potential. In *stage c* (data collection), the surface temperatures of both the membrane and the soil were monitored along with the soil temperature. The latter was measured at three different depths (i.e., 5 cm, 10 cm and 15 cm) for both the field configurations. Finally, *stage d* focused on post-processing and analyzing the dataset about temperature collected during the monitoring campaign. Up to five days that can be considered as representative of the monitored period were defined by varying the percentile from zero to 25, to 50, to 75 and to 100. Then, the attenuation and the phase shift of the thermal wave throughout the soil as well as the cooling potential of the membrane were calculated for each representative day.

2.2. Material Characterization

The highly reflective mulching membrane was 1.5 mm thick, and it consisted of a water-proof membrane (Polyfin Duo® 3015 (www.casali-group.com (accessed on 20 August 2021))) treated with highly reflective pigments. The optical characterization was performed on to the highly reflective layer, while properties reported in Table 1. concern the Polyfin Duo® 3015 membrane and were provided by Polyfin AG company.

Table 1. Technical characteristics of the Polyfin DUO® 3015 membrane.

Technical Characteristics	Testing Methods	Performance
Water vapor transmission property	EN 1931 (B)	120,000
Tensile strength in longitudinal	EN 12311-2 (B)	$\geq 5 \text{ N mm}^{-2}$
Elongation in the longitudinal	EN 12311-2 (B)	$\geq 300\%$
Tear resistance	EN 12 310-2	$\geq 150 \text{ N}$
Dimensional stability	EN 1107-2	$\leq 0.3\%$
Water tightness	ENN 1928 (B)	$\geq 500 \text{ kPa}$

Water resistance property of such a membrane enables collecting rainwater that is exploited for irrigation purposes. A preliminary investigation has already demonstrated that this can positively influence plant growth [14]. Nonetheless, membrane's influences on plant growth cycle and soil humidity are worth further investigation and they will be assessed in future studies.

The optical characterization of the highly reflective membrane utilized in this study focused on the assessment of spectral reflectance, spectral emittance and SRI. The spectral reflectance was assessed through the Solid Spec-3700 spectrophotometer, which was equipped with a 60 mm diameter integrated sphere having a wavelength accuracy of 0.1 nm. According to the ASTM Standard E903-12 [22], the measurement of the spectral near-normal reflectance focused on a wavelength interval ranging between 300 nm and 2500 nm (with a step of 5 nm), while neglecting most of the ultraviolet C spectrum. The spectral reflectance was estimated according to the ASTM Standard G173-03 [23]. Analyses were reiterated three times. Finally, the mean spectral reflectance value was calculated for the ultraviolet (from 250 nm to 400 nm), the visible (from 400 nm to 750 nm), and the infrared spectrum (from 750 nm to 2500 nm), respectively.

Regarding the spectral emittance, it was estimated through the Portable Emissometer AE1 from Device and Services Company. Both the calibration of the apparatus and the evaluation of the material's spectral emittance were conducted in accordance with the ASTM Standard C1371-04a [24]. As before, analyses were reiterated three times.

The SRI was calculated by combining the spectral reflectance and the spectral emittance values, basing on the ASTM Standard E1980-11 [25]. Therefore, the following equation for the calculation of the SRI in standard conditions (air temperature of 310 K, sky temperature of 300 K, and global solar irradiation of 1000 W m^{-2}) was used:

$$SRI = 123.97 - 141.35\chi + 9.655\chi^2 \quad (1)$$

$$\chi = \frac{((1-r) - 0.029\varepsilon)(8.797 + h_c)}{9.5205\varepsilon + h_c} \quad (2)$$

where r is the solar reflectance, ε is the spectral emittance, and h_c is the convection coefficient, which can be considered as high as $5 \text{ Wm}^{-2}\text{K}^{-1}$ or $12 \text{ Wm}^{-2}\text{K}^{-1}$ or $30 \text{ Wm}^{-2}\text{K}^{-1}$, in accordance with the ASTM Standard E1980-11 [25].

2.3. Experimental Field

The experimental field covered a squared area that is 100 m^2 . It was located in the Engineering University Campus in Perugia, Italy. A layer of soil suitable for being cultivated was laid down in the chosen area. The soil consisted of a mixture of sand (60%), clay (20%), humus (10%), and limestone (10%), and it is composed by organic matter (5%), inorganic compounds (45%), voids (25%), and water (25%). The field was arranged into 12 rows where crops could be planted. Up to ten rows were covered by the highly reflective mulching membrane, and a sub-irrigation system ran between the soil and the membrane. The distance between the membrane and the soil was 5 cm. The other two rows (considered as the *reference case*) were equipped with a conventional drip irrigation system, without the mulching membrane. The inclination of the ground together with the water-resistance feature of the membrane permitted rainwater to be recovered into a 5000 L tank during the precipitation events. Such a water volume can be used for irrigation to reduce the exploitation of water from the aquifer.

2.4. Sensors Layout and Data Collection

The monitoring campaign was conducted between 16 March and 10 May 2021. Up to nine type-T thermocouples were used to monitor the surface temperature of both the sides of the membrane (Cool_tout upwards, Cool_Tin downwards) and the soil (Ref_Tout), as well as the soil temperature at 5 cm (Ref_T5, Cool_T5), 10 cm (Ref_T10, Cool_T10) and 15 cm (Ref_T15, Cool_T15) below the surface, for the *reference case* and the *enhanced scenario*. The thermocouples were connected to a Lutron BTM-4208SD data-logger, which recorded the temperature values with a two-minute time-step. Environmental monitoring was performed through a fixed weather station settled in the same university campus. Data concerning air temperature were collected every ten minutes. An overview of the layout of the sensors is presented in Figure 1.

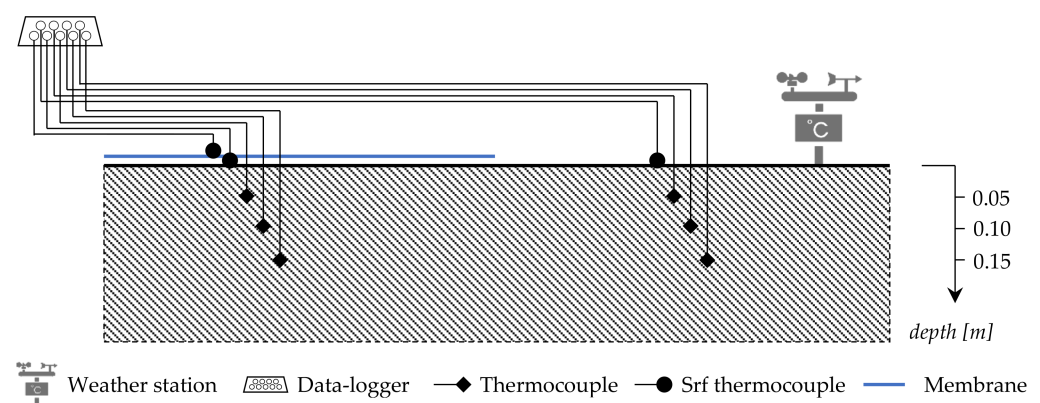


Figure 1. Overview of the layout of the sensors.

2.5. Data Post-Processing

A routing was implemented in MatLab environment for aggregating data that had been recorded with a two-minute time-step (ten-minute time-step for the air temperature) during the monitoring campaign into hourly average values. Five statistical days were defined by varying the percentile of hourly temperature values from zero to 25, to 50, to 75 and to 100.

Moreover, the routine allowed for calculating of key performance indicators (KPIs), such as the attenuation and the phase shift of the thermal wave throughout the soil as well as the cooling potential of the membrane for each day. The attenuation here was assessed as the thermal variation from the soil surface temperature for the *reference case* and from membrane surface temperature for the *enhanced scenario*. To assess the phase shift, first, the distribution of the hourly temperature values throughout the day was determined for each thermocouple. Second, the variation in the time of the peak difference between the peaks was calculated with respect to the surface levels. Regarding the cooling potential, this was defined as the thermal variation between the *reference case* and the *enhanced scenario*, calculated for each pair of thermocouples (located at the same depth). Thus, the cooling potential of the membrane was determined at the surface level and also at 5 cm, 10 cm and 15 cm of depth.

3. Results

3.1. Optical Characterization of the Membrane

Measured spectral reflectance values of the highly reflective membrane are represented in Figure 2, together with the error associated with the nominal value. Table 2 shows the mean values calculated for each wavelength interval (ultraviolet, visible, infra-red). The sample was capable of reflecting most of the visible radiation spectrum while absorbing a considerable amount of radiation within the infrared range as well as almost the totality of ultraviolet radiation spectrum. In particular, the average spectral reflection value estimated in the ultraviolet spectrum equaled $11.35 \pm 0.10\%$, while in the infrared wavelength interval and in the visible range, the average spectral reflectance was $55.25 \pm 0.10\%$ and $82.70 \pm 0.05\%$, respectively. Globally, the membrane was capable of reflecting up to $72.75 \pm 0.08\%$ of the incident solar radiation.

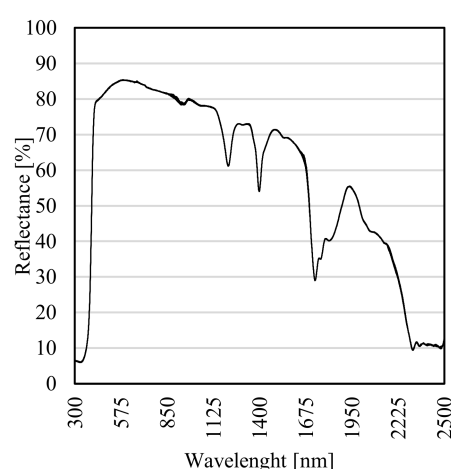


Figure 2. Measured spectral reflectance values with the associated error of the highly reflective membrane.

Table 2. Measured spectral reflectance values for the UV, visible, and IR spectra.

Wavelength Interval	Spectral Reflectance	
	Nominal Value	Error
UV	11.35%	0.10%
Visible	82.70%	0.05%
IR	55.25%	0.10%

Regarding the emittance, the highly reflective mulching membrane was found capable of emitting up to 0.89 ± 0.02 . Following this, the SRI was calculated (Table 3). It was around 90 for every h_c value ($5 \text{ Wm}^{-2}\text{K}^{-1}$, $12 \text{ Wm}^{-2}\text{K}^{-1}$, and $30 \text{ Wm}^{-2}\text{K}^{-1}$).

Table 3. Estimated values for the SRI coefficient, according to ASTM Standard E1980-11.

h_c [$\text{Wm}^{-2}\text{K}^{-1}$]	SRI	
	Nominal Value	Error
5	89.15	0.85
12	89.45	0.60
30	89.70	0.40

3.2. Monitoring Campaign

Results from the monitoring campaign are presented in this subsection (Figure 3) focusing on three series of seven consecutive days that can be considered as representative of weeks showing the lowest average air temperature (coolest week), the highest average air temperature (warmest week), and the most intense precipitation (mostly rainy week), that occurred in the monitoring period.

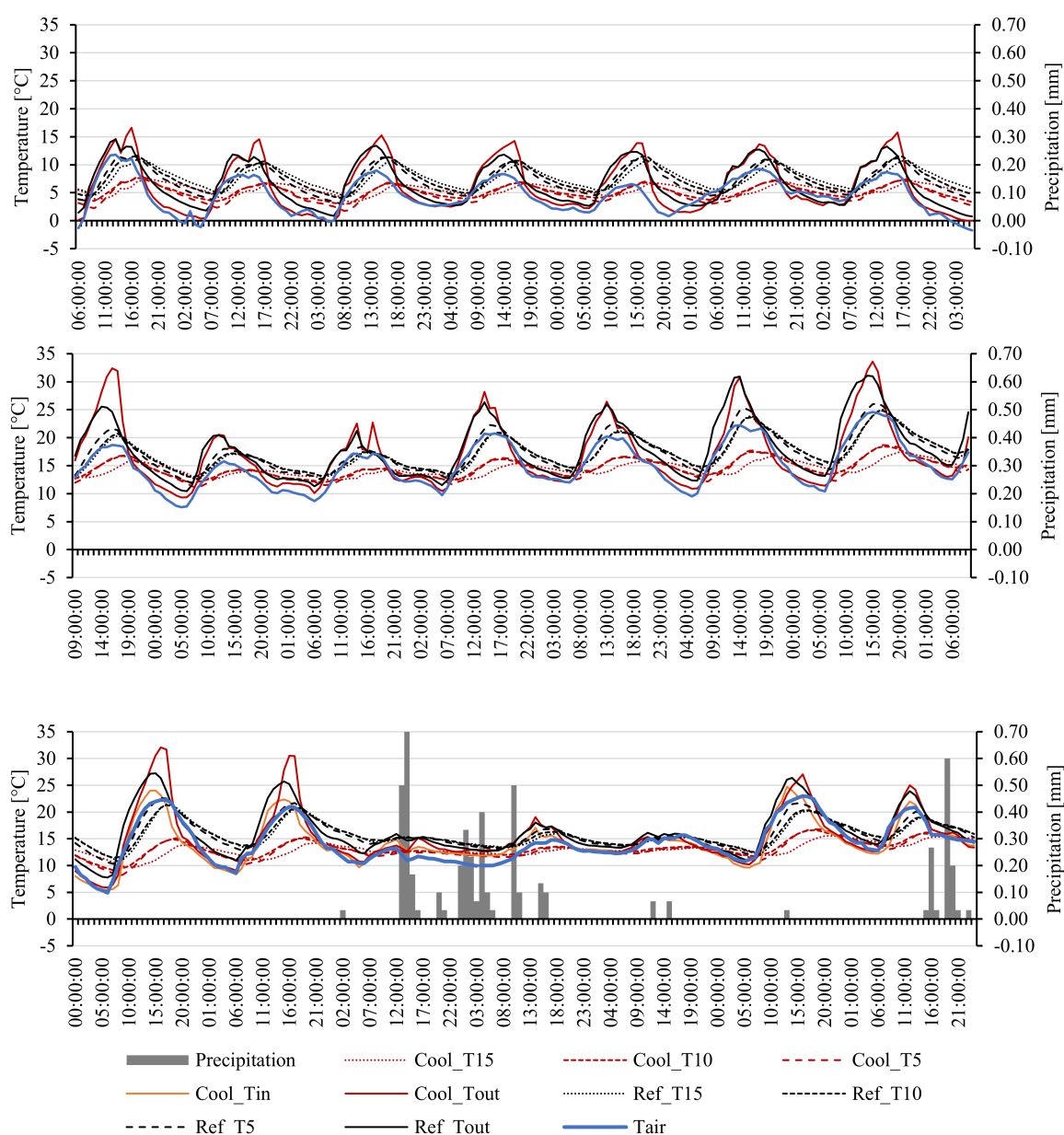


Figure 3. From the top, monitored data for the coolest week (from 17 March at 6.00 a.m. until 24 March at 6.00 a.m.), the warmest week (from 3 May at 9.00 a.m. until 10 May at 9.00 a.m.), and the mostly rainy week (from 25 April at 0.00 a.m. until 2 May at 0.00 a.m.).

The coolest week started on 17 March at 6.00 a.m. and ended on 24 March at 6:00 a.m., and the average air temperature was as high as 4.5 °C. The warmest week started on 3 May at 9.00 a.m. and ended on 10 May at 9.00 a.m., with an average air temperature equal to 15.1 °C. Finally, the mostly rainy week started on 25 April at 0.00 a.m. and ended on 2 May at 0.00 a.m. The accumulated precipitation over the seven days was 5.13 mm.

3.3. Statistical Analysis and KPIs' Calculation

The five statistical days corresponding to the 0th, the 25th, the 50th, the 75th, and the 100th percentiles of the monitored temperature values were defined (Figure 4) to calculate the KPIs (thermal attenuation, phase shift, cooling potential).

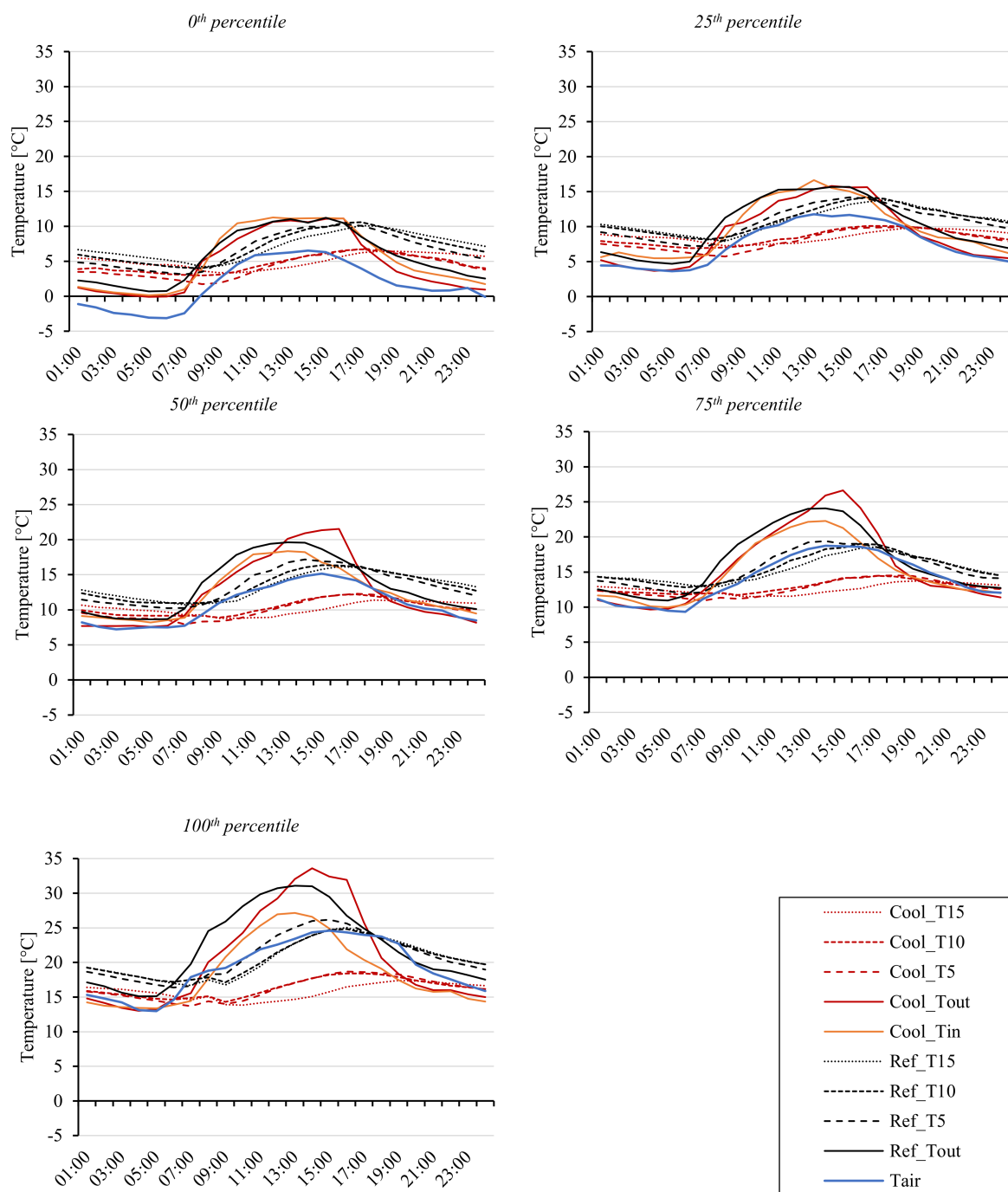


Figure 4. Five statistical days corresponding to the 0th, the 25th, the 50th, the 75th, and the 100th percentiles of the monitored temperature values.

The overview of the calculated KPIs together with the peak temperature (T_{peak}), the hour of the day showing the highest temperature value (HoD_{peak}), and the daily mean temperature ($T_{daily,avg}$) is reported in Table 4 for each percentile. A graphical comparison of the cooling potential of the membrane is presented in Figure 5.

Table 4. Estimated KPIs, T_{peak} , HoD_{peak} , and $T_{daily,avg}$ for each percentile.

Indicator	Cool_T15	Cool_T10	Cool_T5	Cool_Tout	Cool_Tin	Ref_T15	Ref_T10	Ref_T5	Ref_Tout
0th percentile									
T_{peak} [°C]	6.4	6.7	6.8	11.1	11.3	10.1	10.6	10.3	11.2
HoD_{peak} [h]	19	17	17	16	12	17	17	16	15
$T_{daily,avg}$ [°C]	5.0	4.6	4.3	4.6	5.3	7.2	7.0	6.6	5.7
th. attenuation [°C]	−4.7	−4.4	−4.3	-	0.1	−1.1	−0.6	−0.9	-
phase shift [h]	3	1	1	-	−4	2	2	1	-
cooling potential [°C]	−2.1	−2.4	−2.4	−1.0	−0.4	-	-	-	-
25th percentile									
T_{peak} [°C]	9.8	10.1	9.9	15.8	16.6	13.8	14.2	14.2	15.7
HoD_{peak} [h]	19	17	17	14	13	17	16	15	15
$T_{daily,avg}$ [°C]	8.6	8.4	8.0	9.1	9.8	10.9	11.0	10.7	10.2
th. attenuation [°C]	−6.0	−5.7	−5.9	-	0.8	−1.9	−1.5	−1.5	-
phase shift [h]	5	3	3	-	−1	2	1	0	-
cooling potential [°C]	−2.3	−2.6	−2.7	−1.1	−0.4	-	-	-	-
50th percentile									
T_{peak} [°C]	11.4	12.2	12.3	21.5	18.4	16.2	16.4	17.2	19.6
HoD_{peak} [h]	18	17	17	16	13	16	15	14	13
$T_{daily,avg}$ [°C]	10.1	10.3	10.0	12.6	12.5	13.3	13.4	13.4	13.5
th. attenuation [°C]	−10.1	−9.3	−9.2	-	−3.2	−3.5	−3.3	−2.4	-
phase shift [h]	2	1	1	-	−3	3	2	1	-
cooling potential [°C]	−3.2	−3.1	−3.4	−0.9	−1.0	-	-	-	-
75th percentile									
T_{peak} [°C]	13.7	14.5	14.5	26.6	22.3	18.6	19.0	19.4	24.1
HoD_{peak} [h]	19	17	18	15	14	17	16	14	14
$T_{daily,avg}$ [°C]	12.6	12.9	12.6	15.8	15.1	15.4	15.6	15.5	16.5
th. attenuation [°C]	−12.9	−12.2	−12.1	-	−4.4	−5.5	−5.0	−4.7	-
phase shift [h]	4	2	3	-	−1	3	2	0	-
cooling potential [°C]	−2.8	−2.7	−2.9	−0.7	−1.4	-	-	-	-
100th percentile									
T_{peak} [°C]	17.4	18.4	18.7	33.6	27.2	25.0	24.8	26.2	31.1
HoD_{peak} [h]	19	16	16	14	13	16	16	15	13
$T_{daily,avg}$ [°C]	15.8	16.3	16.2	20.7	18.5	20.4	20.5	20.8	22.4
th. attenuation [°C]	−16.2	−15.2	−14.9	-	−6.4	−6.0	−6.3	−4.9	-
phase shift [h]	5	2	2	-	−1	3	3	2	-
cooling potential [°C]	−4.6	−4.2	−4.6	−1.7	−3.8	-	-	-	-

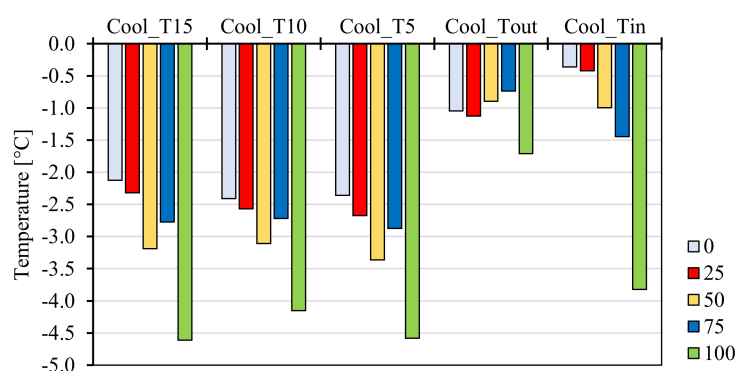


Figure 5. Comparison of the cooling potential of the membrane at different depths.

The surface peak temperature of the membrane ranged from 11.1 °C (0th percentile) to 33.6 °C (100th percentile). Similarly, the surface peak temperature of the soil varied between 11.2 °C (0th percentile) and 31.1 °C (100th percentile). Evapotranspiration phenomena,

which take place in the monitored permeable surface, were as effective as the membrane in cooling the surface temperature. However, the membrane enables a greater attenuation of the thermal wave throughout the soil. At 15 cm of depth, the temperature is reduced from the surface temperature by a quantity ranging from $-4.7\text{ }^{\circ}\text{C}$ (0th percentile) to $-16.2\text{ }^{\circ}\text{C}$ (100th percentile) in the *enhanced scenario*; and from $-1.1\text{ }^{\circ}\text{C}$ (0th percentile) to $-6.0\text{ }^{\circ}\text{C}$ (100th percentile) in the *reference case*. A similar trend is shown at the other depths (10 cm and 5 cm below the surface).

Regarding the phase shifting, the mulching membrane is demonstrated to retard the temperature peaks by up to two hours in addition to the capability of the soil. Thus, the soil from the *enhanced scenario* is maintained at cool for a longer period throughout the daytime if compared to the *reference case*.

As far as the cooling potential of the membrane is concerned, the post-processed temperature values highlighted that the soil temperature in the *enhanced scenario* was always lower than in the *reference case* for each percentile. Furthermore, the variation was almost constant when moving from 5 to 10 cm, and to 15 cm depth. A temperature reduction within the soil (Cool_T15, Cool_T10, and Cool_T5) as high as $-2.2\text{ }^{\circ}\text{C}$ (the lowest) was observed for the 0th percentile, while a value equal to $-4.4\text{ }^{\circ}\text{C}$ (the highest) was found for the 100th percentile. As mentioned before, the highly reflective mulching membrane was not capable of significantly cooling down the membrane surface facing the sky dome (Cool_Tout) as well as the surface facing the soil (Cool_Tin).

4. Discussion

Results demonstrate that the highly reflective mulching membrane can reduce from the *reference case* both the surface and soil temperature by around 1 and $3\text{ }^{\circ}\text{C}$ (50th percentile), respectively. Furthermore, higher thermal attenuation and phase shift were enabled by the highly reflective mulching membrane used in the experimental facility. Soil temperature is a primary factor that affects the rate of plant development. Thus, achieving lower temperature values within the soil will allow partial mitigation of the effects of temperature extremes on plant growth such as the drop in grain yield (up to -90%) in maize crops when warmer temperatures are experienced [26].

Alongside this, a cooler surface (membrane was averagely $1\text{ }^{\circ}\text{C}$ cooler than the ground) emits a lower amount of energy according to the Stefan-Boltzmann Law. Considering a spectral emittance of 0.95 for the ground, the reduction in the emitted energy varied from $-3.4\text{ }10^{-5}\text{ W m}^{-2}$ (0th percentile) to $-4.2\text{ }10^{-3}\text{ W m}^{-2}$ (100th percentile), with an average value of $-5.4\text{ }10^{-4}\text{ W m}^{-2}$. The optical properties of the membrane allow greater amounts of solar irradiation to be reflected without altering its wavelength. Such a phenomenon contributes to mitigate global warming by modifying the Earth thermal balance, which involves solar irradiance, chemical composition of the atmosphere, and both ground and water properties. Hence, an amount of avoided carbon emissions can be assigned to the global warming mitigation potential of the highly reflective membrane as described in [13]. Following this, the experimental field in Perugia can be offset by up to 10 tCO_{2-eq} after 20 years from the installation of the membrane.

A few observations can be made on the methodology followed in this study. First, assessing different percentiles instead of the mean quantity permits to better investigate the influences of the mulching membrane, particularly when monitored parameters refer to temperature values. Second, the results highlighted that it is not necessary to place thermocouple sensors at three different depths that are near each other when evaluating the thermal attenuation and the cooling potential. Indeed, the collected information about temperature was similar and redundant. However, assessing three depths was necessary for the quantification of the phase shift indicator.

As far as future developments are concerned, the monitoring campaign will investigate other parameters, such as soil humidity, and it will be performed for longer periods to evaluate the effects of seasonality on the membrane's performances. Different membranes will be tested to compare their performances. Finally, the influences of food crops on the

three KPIs should be investigated in the future: the optical behavior of the membrane may be altered by leaf coverage and the consequent shadowing.

5. Conclusions

The influences on heat propagation throughout the soil of a system based on a highly reflective mulching membrane were investigated focusing on thermal attenuation, phase shifting and cooling potential indicators. A monitoring campaign was conducted to collect data concerning surface and soil temperature; then, a statistical approach was followed to post-process this information. The membrane was demonstrated to be capable of increasing the thermal attenuation and the phase shifting of the thermal wave throughout the soil, while always decreasing the temperatures from the *reference case*.

The main results are summarized in the following bullet points:

- Negligible variations can be observed between the *enhanced scenario* and the *reference case* in surface temperature throughout the five statistical days;
- The membrane enables a greater attenuation of the thermal wave throughout the soil, which can be up to 16 °C (in 100th percentile) cooler than the membrane's surface;
- Covered soil is on average 3 °C cooler than uncovered soil, with potential benefits for plant growth;
- The highly reflective mulching membrane permits to offset carbon emissions from agriculture activities by around 0.1 tCO₂-eq m⁻², after 20 years from its installation.

Author Contributions: Conceptualization, M.M. and F.C.; methodology, M.M. and A.N.; software, M.M.; validation, F.S., A.N. and F.C.; investigation, M.M. and A.D.G.; resources, F.C.; data curation, M.M. and A.D.G.; writing—original draft preparation, M.M. and A.D.G.; writing—review and editing, A.N., F.S. and F.C.; visualization, M.M.; supervision, F.C. All authors have read and agreed to the published version of the manuscript.

Funding: This research received no external funding.

Institutional Review Board Statement: Not applicable.

Informed Consent Statement: Not applicable.

Data Availability Statement: Not applicable.

Conflicts of Interest: The authors declare no conflict of interest.

References

1. Pachauri, R.K.; Meyer, L.A. *IPCC, 2014: Climate Change 2014: Synthesis Report. Contribution of Working Groups I, II and III to the Fifth Assessment Report of the Intergovernmental Panel on Climate Change*; Pachauri, R.K., Meyer, L.A., Eds.; IPCC: Geneva, Switzerland, 2014; ISBN 978-92-9169-143-2.
2. World Meteorological Organization. *State of the Global Climate 2020*; World Meteorological Organization: Geneva, Switzerland, 2021.
3. European Environment Agency. *Total Greenhouse Gas Emission Trends and Projections in Europe*; European Environment Agency: Copenhagen, Danish, 2019.
4. Clune, S.; Crossin, E.; Verghese, K. Systematic review of greenhouse gas emissions for different fresh food categories. *J. Clean. Prod.* **2017**, *140*, 766–783. [[CrossRef](#)]
5. Tukker, A.; Jansen, B. Environmental Impacts of Products: A Detailed Review of Studies. *J. Ind. Ecol.* **2006**, *10*, 159–182. [[CrossRef](#)]
6. Vitasse, Y.; Bottero, A.; Cailleret, M.; Bigler, C.; Fonti, P.; Gessler, A.; Lévesque, M.; Rohner, B.; Weber, P.; Rigling, A.; et al. Contrasting resistance and resilience to extreme drought and late spring frost in five major European tree species. *Glob. Chang. Biol.* **2019**, *25*, 3781–3792. [[CrossRef](#)] [[PubMed](#)]
7. Ma, Q.; Huang, J.-G.; Hänninen, H.; Berninger, F. Divergent trends in the risk of spring frost damage to trees in Europe with recent warming. *Glob. Chang. Biol.* **2019**, *25*, 351–360. [[CrossRef](#)] [[PubMed](#)]
8. Garnett, T. *Fruit and Vegetables & UK Greenhouse Gas Emissions: Exploring the Relationship*; Work of the Food Climate Research Network: Guildford, UK, 2006.
9. Caracciolo, F.; Cicia, G.; Del Giudice, T.; Menna, I.; Cembalo, L. CO₂ Emission in the Fresh Vegetables Chains: A meta-analysis. *Proc. Syst. Dyn. Innov. Food Netw.* **2013**, *14*, 96–102.
10. Hudu, A.I.; Futuless, K.N.; Gworgwor, N.A. Effect of Mulching Intensity on the Growth and Yield of Irrigated Tomato (*Lycopersicon esculentum* Mill.) and Weed Infestation in Semi-Arid Zone of Nigeria. *J. Sustain. Agric.* **2002**, *21*, 37–45. [[CrossRef](#)]

11. Mahmood, M.; Farooq, K.; Amjad, H.; Raham, S. Effect of Mulching on Growth and Yield of Potato Crop. *Asian J. Plant Sci.* **2002**, *2*. [\[CrossRef\]](#)
12. Manni, M.; Coccia, V.; Cavalaglio, G.; Nicolini, A.; Petrozzi, A. Best practices for recovering rural abandoned towers through the installation of small-scale biogas plants. *Energies* **2017**, *10*, 1224. [\[CrossRef\]](#)
13. Manni, M.; Petrozzi, A.; Coccia, V.; Nicolini, A.; Cotana, F. Investigating alternative development strategies for sport arenas based on active and passive systems. *J. Build. Eng.* **2020**, *31*, 101340. [\[CrossRef\]](#)
14. Manni, M.; Di Giuseppe, A.; Petrozzi, A.; Nicolini, A.; Rossi, F.; Cotana, F. High-reflective Mulching Membrane for a Sustainable Development: Monitoring Campaign. *E3S Web Conf.* **2020**, *197*, 8012. [\[CrossRef\]](#)
15. Manni, M.; Lobaccaro, G.; Goia, F.; Nicolini, A.; Rossi, F. Exploiting selective angular properties of retro-reflective coatings to mitigate solar irradiation within the urban canyon. *Sol. Energy* **2019**, *189*, 74–85. [\[CrossRef\]](#)
16. Yuan, J.; Emura, K.; Farnham, C.; Sakai, H. Application of glass beads as retro-reflective facades for urban heat island mitigation: Experimental investigation and simulation analysis. *Build. Environ.* **2016**, *105*, 140–152. [\[CrossRef\]](#)
17. Rossi, F.; Castellani, B.; Presciutti, A.; Morini, E.; Anderini, E.; Filipponi, M.; Nicolini, A. Experimental evaluation of urban heat island mitigation potential of retro-reflective pavement in urban canyons. *Energy Build.* **2016**, *126*, 340–352. [\[CrossRef\]](#)
18. Piselli, C.; Pisello, A.L.; Saffari, M.; Gracia, A.d.; Cotana, F.; Cabeza, L.F. Cool Roof Impact on Building Energy Need: The Role of Thermal Insulation with Varying Climate Conditions. *Energies* **2019**, *12*, 3354. [\[CrossRef\]](#)
19. Pisello, A.L.; Castaldo, V.L.; Taylor, J.E.; Cotana, F. Expanding Inter-Building Effect modeling to examine primary energy for lighting. *Energy Build.* **2014**, *76*, 513–523. [\[CrossRef\]](#)
20. Pisello, A.L.; Taylor, J.E.; Xu, X.; Cotana, F. Inter-building effect: Simulating the impact of a network of buildings on the accuracy of building energy performance predictions. *Build. Environ.* **2012**, *58*, 37–45. [\[CrossRef\]](#)
21. Rossi, F.; Pisello, A.L.; Nicolini, A.; Filipponi, M.; Palombo, M. Analysis of retro-reflective surfaces for urban heat island mitigation: A new analytical model. *Appl. Energy* **2014**, *114*, 621–631. [\[CrossRef\]](#)
22. ASTM International ASTM E903-12. *Standard Test Method for Solar Absorptance, Reflectance, and Transmittance of Materials Using Integrating Spheres* 2012; ASTM: West Conshohocken, PA, USA, 2012.
23. ASTM International ASTM G173-03. *Standard Tables for Reference Solar Spectral Irradiances: Direct Normal and Hemispherical on 37° Tilted Surface* 2020; ASTM: West Conshohocken, PA, USA, 2020.
24. ASTM International ASTM C1371-04a. *Standard Test Method for Determination of Emittance of Materials Near Room Temperature Using Portable Emissometers* 2004; ASTM: West Conshohocken, PA, USA, 2004.
25. ASTM International ASTM E1980-11. *Standard Practice for Calculating Solar Reflectance Index of Horizontal and Low-Sloped Opaque Surfaces* 2019; ASTM: West Conshohocken, PA, USA, 2019.
26. Hatfield, J.L.; Prueger, J.H. Temperature extremes: Effect on plant growth and development. *Weather Clim. Extrem.* **2015**, *10*, 4–10. [\[CrossRef\]](#)